The current issue and full text archive of this journal is available at
www.emeraldinsight.com/0961-5539.htm

A simple and robust linear eddy-viscosity formulation for curved and rotating flows

William D. York
Department of Mechanical Engineering, Clemson University, Clemson, South Carolina, USA
D. Keith Walters
Department of Mechanical Engineering, Mississippi State University, Starkville, Mississippi, USA, and
James H. Leylek
Department of Mechanical Engineering, Clemson University, Clemson, South Carolina, USA

Received 19 November 2007
Revised 10 April 2008
Accepted 6 May 2008

Abstract

Purpose – The purpose of this paper is to present a new eddy-viscosity formulation designed to exhibit a correct response to streamline curvature and flow rotation. The formulation is implemented into a linear k-ε turbulence model with a two-layer near-wall treatment in a commercial computational fluid dynamics (CFD) solver.

Design/methodology/approach – A simple, robust formula is developed for the eddy-viscosity that is curvature/rotation sensitive and also satisfies realizability and invariance principles. The new model is tested on several two- and three-dimensional problems, including rotating channel flow, U-bend flow and internally cooled turbine airfoil conjugate heat transfer. Predictions are compared to those with popular eddy-viscosity models.

Findings – Converged solutions to a variety of turbulent flow problems are obtained with no additional computational expense over existing two-equation models. In all cases, results with the new model are superior to two other popular k-ε model variants, especially for regions in which rapid rotation or strong streamline curvature exists.

Research limitations/implications – The approach adopted here for linear eddy-viscosity models may be extended in a straightforward manner to non-linear eddy-viscosity or explicit algebraic stress models.

Practical implications – The new model is a simple "plug-in" formula that contains important physics not included in most linear eddy-viscosity models and is easy to implement in most flow solvers.

Originality/value – The present model for curved and rotating flows is developed without the need for second derivatives of velocity in the formulation, which are known to present difficulties with unstructured meshes.

Keywords Fluid dynamics, Turbulence, Modelling, Heat transfer

Paper type Research paper

Nomenclature

C_f	skin friction coefficient	k	turbulent kinetic energy $= \frac{1}{2}\overline{u_i u_i}$ [m^2/s^2]
C_μ	eddy-viscosity coefficient	L	characteristic length, total surface arc length [m]
c_p	specific heat [J/kg K]	n	normal distance to surface or boundary [m]
H	channel height [m]	P^k	production of turbulent kinetic energy
h_c	convective heat transfer coefficient [W/m^2 K]		

International Journal of Numerical Methods for Heat & Fluid Flow
Vol. 19 No. 6, 2009
pp. 745-776

0961-5539
DOI 10.1108/09615530910972995

Pr	Prandtl number
Re_H, Re_c	Reynolds number
Re_y	turbulent Reynolds number for near-wall turbulence model = $\frac{\sqrt{k} \cdot y}{\nu}$
Re_τ	turbulent Reynolds number for wall-bounded flow = $\frac{u * h}{\nu}$
Ro	rotation number = $\frac{\omega_m H}{U_m}$
s	distance along vane surface from leading edge [m]
S	strain-rate magnitude = $\sqrt{2S_{ij}S_{ij}}$
S_{ij}	rate-of-strain tensor = $\frac{1}{2}\left(\frac{\partial U_i}{\partial x_j} + \frac{\partial U_j}{\partial x_i}\right)$ [s^{-1}]
St	Stanton number = $\frac{h_c}{\rho c_p U_{ref}}$
t	time [s]
t^*	normalized time, $S \cdot t$
T	temperature [K]
TL	turbulence level = $100 \cdot \sqrt{2k/3}/U_\infty$ [percent]
u, v, w	velocity components in the x, y, and z directions, respectively [m/s]
U	mean velocity component (with i, j, k indices), velocity magnitude [m/s]
U^+	normalized velocity in boundary layer = U/u^*
u^*	wall friction velocity = $\sqrt{\tau_w/\rho}$ [m/s]
v	velocity scale [m/s]
W	modified flow rotation-rate magnitude = $\sqrt{2W_{ij}W_{ij}}$ [s^{-1}]
W_{ij}	modified flow rotation-rate tensor [s^{-1}]
x, y, z	cartesian coordinate directions
y^+	non-dimensional wall distance in turbulent boundary layer
ε	dissipation rate of turbulent kinetic energy [m^2/s^3]
κ	von Karman constant
μ	dynamic viscosity [N s/m^2]
μ_T	turbulent (eddy) viscosity [N s/m^2]
ν	kinematic viscosity [m^2/s]
ρ	density [kg/m^3]
θ	dimensionless temperature = $(T - T_c)/(T_0 - T_c)$, angle in U-bend
τ_w	wall shear stress [N/m^2]
ω	specific dissipation rate of turbulence [s^{-1}]
ω_m	angular velocity of reference frame relative to inertial frame [s^{-1}]
Ω	rotation-rate magnitude = $\sqrt{2\Omega_{ij}\Omega_{ij}}$ [s^{-1}]
Ω_{ij}	rotation-rate tensor in inertial frame = $\frac{1}{2}\left(\frac{\partial U_i}{\partial x_j} - \frac{\partial U_j}{\partial x_i}\right)$ [s^{-1}]
Ω'_{ij}	rotation-rate tensor in rotating frame [s^{-1}]

Subscripts

c	coolant air total (stagnation) condition, based on airfoil chord length
i, j, k	indices used in tensor notation
LE	at airfoil leading edge plane
m	mean value over channel cross-section
PS	vane pressure surface
ref	condition at reference location
SS	vane suction surface
T	turbulent
TE	at airfoil trailing edge plane
w	from wall or condition at surface
∞	inlet or freestream condition
0	total (stagnation)

Operators

~(overbar) instantaneous	e_{ijk}	tensor permutation operator
–(overbar) ensemble or time average	δ_{ij}	kronecker delta

Introduction

Computational fluid dynamics (CFD) has emerged as a recognized, predictive tool for analysis of increasingly complicated fluid flow and heat transfer problems. In many applications, CFD may greatly reduce product development time and cost, especially in situations where several different design iterations are evaluated. For most engineering problems, a CFD simulation based on solution of the Reynolds-averaged Navier–Stokes equations is currently the most viable option considering accuracy and numerical cost.

As a consequence of Reynolds-averaging, the gradient of the turbulent stress tensor, $\overline{\tilde{\rho}u_i u_j}$, appears in the momentum equations. A turbulence model is used to relate the unknown turbulent stresses to known quantities, closing the system of equations. As the fidelity of numerical simulation tools has increased, the quality of the numerical predictions is often limited by the performance of the turbulence model. In many cases, as assumptions are made to arrive at economic models, sensitivity to complex physical mechanisms is reduced or eliminated. One such example is the sensitivity of many models to streamline curvature and rotation.

Strong or even moderate curvature can significantly impact the turbulence field (Bradshaw, 1973), which will in turn influence the mean flow development. Correct response to curvature and/or rotational effects by the turbulence model is therefore critical. From a design point-of-view, the quality of predictions of wall shear stress or heat transfer coefficient on curved surfaces may be significantly influenced by the model's response, or lack thereof, to curvature or rotation. For example, it is well documented in the literature that convex curvature is stabilizing and suppresses turbulence levels, while concave curvature is destabilizing and tends to augment turbulence (Muck *et al.*, 1985; Hoffman *et al.*, 1985).

Differential Reynolds-stress turbulence models solve a transport equation for the six unique turbulent stress components, and they naturally contain sensitivity to streamline curvature and reference frame rotation through the exact form of the production terms (Speziale and Mac Giolla Mhuiris, 1989). Yet models of this class are computationally expensive, and their equations tend to be numerically stiff, traits that make them non-ideal for a design environment (Pettersson Reif *et al.*, 1999). To date, the "workhorse" models in industry are the eddy-viscosity class of models, which follow the Boussinesq assumption relating the turbulent stress components to the mean strain rate via a turbulent- or eddy-viscosity. Popular models in this class are the k-ε and k-ω models, which represent a reasonable compromise between expense and physical realism in many flows. However, the "standard" k-ε model (Launder and Spalding, 1972) and k-ω model (Wilcox, 1988), as well as most variants, lack any explicit sensitivity to streamline curvature and/or reference frame rotation. This can lead to significant error in computational predictions in many flow situations.

For more than three decades researchers have attempted to incorporate rotation and curvature corrections into linear eddy-viscosity models (Launder *et al.*, 1977; Howard *et al.*, 1980; Leschziner and Rodi, 1981; Gooray *et al.*, 1985; Park and Chung, 1989). These attempts were shown to successfully improve prediction in the flows for which they were tested, however they were based on *ad hoc* modifications and, more importantly, did not typically satisfy mathematical invariance principles.

As an extension of Boussinesq-based models, both algebraic stress models and so-called non-linear eddy-viscosity models have been developed. Some authors have reported an improvement over linear models in their ability to resolve curvature effects, even when no explicit sensitization to flow rotation and/or curvature has been incorporated (Iacovides *et al.*, 1996; Song *et al.*, 2001; Yang and Ma, 2003). In addition, some forms of these models have been explicitly sensitized to rotation and curvature, resulting in further improvement to their predictive capability (Girimaji, 1997; Rumsey and Gatski, 2001; Fu and Qian, 2002; Wallin and Johansson, 2002; Hellsten, 2002; Grundestam *et al.*, 2005; Wang and Thangam, 2006). Significantly, the curvature corrections in these recent models have been based primarily on mathematically consistent application of invariance and frame indifference principles, in contrast to the *ad hoc* modifications found in earlier attempts.

There have been far fewer documented efforts to appropriately sensitize linear eddy-viscosity models to the effects of rotation and curvature. Two notable exceptions are the development of curvature-corrected versions of the model by Spalart and Allmaras (1992) and the v2-f model by Durbin (1991). Spalart and Shur (1997) introduced an invariant-based curvature correction to the former, which was subsequently shown to yield improved results over the original model for several test cases (Shur *et al.*, 2000). Similarly, Pettersson Reif *et al.* (1999) demonstrated improved predictive capability of a curvature-corrected v2-f model.

This paper presents the development of a new formulation for the eddy viscosity intended for use in the general class of two-equation turbulence models, as a simple modification that incorporates rotation and curvature effects. Specifically, the eddy-viscosity coefficient C_μ is formulated to reproduce the proper response to streamline curvature and/or reference frame rotation, yielding a curvature-corrected linear eddy-viscosity model, in contrast to the non-linear model forms that have recently been proposed. The new formulation may be easily implemented into existing flow solvers that incorporate RANS-based eddy-viscosity turbulence models. The new form of the eddy viscosity is Galilean invariant, frame indifferent and satisfies the realizability constraint on the Reynolds-stress tensor. As used in this paper, Galilean invariance refers to the property that a model yields identical results when cast into any inertial reference frame. Frame indifference refers to the property that a model yields identical results when cast into either an inertial or non-inertial (rotating) reference frame. It is possible, of course, to develop models that satisfy one of these conditions without satisfying the other. The new model avoids the use of second derivatives of the velocity field in defining the local flow rotation by adopting a simpler approximation to rotation based only on local strain and rotation-rate magnitude. The importance of the flow rotation, as distinct from vorticity or reference frame rotation, is discussed, and the analogy between curved flows and rotating flows is highlighted.

The new eddy-viscosity formula has been implemented into a two-layer k-ε model for purposes of demonstration and validation. The model solves equations for turbulent kinetic energy (k) and dissipation rate (ε) in the far-field, while solving only the k equation near the wall and prescribing a length scale based on wall distance. The interface between the near-wall region and the far-field is evaluated based on the smaller of the two length scales determined by either the wall distance or the dissipation rate.

In the current work, the new model form is tested on several problems where curvature or rotation is an important mechanism influencing the Reynolds stress and mean flow. These include rotating homogenous shear flow, rotating fully developed

channel flow and two-dimensional flow in a U-bend. Numerical predictions are compared to experimental data and direct numerical simulations (DNSs) or large eddy simulations in terms of mean flow and turbulence development. Finally, to demonstrate the model in a realistic design application, the new model is employed in a conjugate heat transfer simulation of an internally cooled gas turbine vane. Since the vane external surfaces are highly curved in some regions, this complex simulation should benefit from a turbulence model with curvature sensitivity, allowing more accurate prediction of external heat transfer coefficient.

Model development

This section describes the procedure and assumptions in the development of the new eddy-viscosity formulation. The model is designed to include the effects of streamline curvature on the turbulence structure, and, by analogy, also reproduce the effects of system rotation. As stated earlier, the approach is based on the Boussinesq approximation, which has the advantages of linearity with respect to the mean strain tensor, tensor invariance and reference frame indifference (when the eddy-viscosity definition is also frame indifferent). Additionally, this approach is simple to implement into existing models and generally stable during the solution process for nearly all problems.

As a starting point, we consider the Reynolds-stress tensor decomposed as

$$\overline{u_i u_j} = \left(b_{ij} + \frac{2}{3}\delta_{ij} \right) k, \tag{1}$$

where b_{ij} is the anisotropy tensor, whose components indicate the magnitude of departure from isotropic turbulence, and k is the turbulent kinetic energy. For the class of models considered here, k is determined from the solution of a model transport equation. The anisotropy tensor is determined from the mean strain rate using the Boussinesq hypothesis:

$$b_{ij} = -\frac{\mu_T}{\rho k}\left(\frac{\partial U_i}{\partial x_j} + \frac{\partial U_j}{\partial x_i} \right) + \frac{2}{3}\left(\frac{\mu_T}{\rho k}\frac{\partial U_k}{\partial x_k} \right)\delta_{ij}. \tag{2}$$

The eddy viscosity, μ_T, incorporates additional physical effects, such as wall damping or, relevant to the current work, curvature and rotation. The general expression for the eddy viscosity is:

$$\mu_T = f_\mu C_\mu \rho \sqrt{k} \ell_T. \tag{3}$$

The turbulent length scale is determined for the k-ε model as $\ell_T \sim k^{3/2}/\varepsilon$, for the k-ω model as $\ell_T \sim k^{1/2}/\omega$, and for the algebraic near-wall model of Wolfstein (1969) adopted here as $\ell_T \sim C_L y$, where y is the distance to the nearest wall. The damping function f_μ incorporates the effects of near-wall viscous damping and is specific to the particular model variant. Following convention, the term "linear eddy-viscosity" is used to describe the current model since Equation (2) indicates that the anisotropy tensor is proportional to the strain-rate tensor, in contrast to non-linear models for which the anisotropy tensor includes higher-order constructions of S_{ij} and/or Ω_{ij}. Note, however, that the scalar proportionality coefficient (i.e. the eddy viscosity) may include scalar invariants of the strain and rotation-rate tensors in its computation. "Linear

eddy-viscosity" also indicates that the current model will yield isotropic normal Reynolds-stress components in two-dimensional shear flow.

Gatski and Speziale (1993) presented an explicit algebraic stress model for b_{ij} based on a modified form of the differential Reynolds-stress model of Speziale *et al.* (1991) and the assumption of local structural equilibrium, also referred to as weak equilibrium. The result is:

$$b_{ij} = \frac{\left(\frac{4}{3} - C_2\right)}{(C_3 - 2)} \cdot \frac{6}{3 - 2\eta^2 + 6\zeta^2} \cdot \left[S^*_{ij} + \left(S^*_{ik} W^*_{kj} + S^*_{jk} W^*_{ki} \right) - 2\left(S^*_{ik} S^*_{kj} - \frac{1}{3} S^*_{kl} S^*_{kl} \delta_{ij} \right) \right], \tag{4}$$

where

$$\eta^2 = S^*_{ij} S^*_{ij}, \tag{5}$$

$$\zeta^2 = W^*_{ij} W^*_{ij}, \tag{6}$$

$$S^*_{ij} = \frac{1}{2} g \frac{k}{\varepsilon} (2 - C_3) S_{ij}, \tag{7}$$

$$W^*_{ij} = \frac{1}{2} g \frac{k}{\varepsilon} (2 - C_4) W_{ij}, \tag{8}$$

$$W_{ij} = \Omega'_{ij} + \frac{(C_4 - 4)}{(C_4 - 2)} e_{mji} \omega_m, \tag{9}$$

$$g = \left(\frac{1}{2} C_1 + \frac{P^k}{\varepsilon} - 1 \right)^{-1}. \tag{10}$$

Note that S_{ij} and Ω'_{ij} represent the strain rate and the rotation rate expressed in a reference frame rotating with angular velocity ω_m:

$$S_{ij} = \frac{1}{2} \left(\frac{\partial U_i}{\partial x_j} + \frac{\partial U_j}{\partial x_i} \right), \tag{11}$$

$$\Omega'_{ij} = \frac{1}{2} \left(\frac{\partial U_i}{\partial x_j} - \frac{\partial U_j}{\partial x_i} \right). \tag{12}$$

The constants C_1–C_4 are directly related to the constants appearing in the model terms of the original differential Reynolds-stress model. Gatski and Speziale (1993) derived an explicit formulation by assuming that the production-to-dissipation ratio that appears in Equation (10) can be accurately represented using a constant value, equal to a universal value for shear driven homogeneous turbulence at structural equilibrium. In addition, *ad hoc* regularization procedures (Gatski and Speziale, 1993; Abid *et al.*, 1996) have been incorporated to eliminate the singularity arising in Equation (4) for large values of η.

Equation (4) may be utilized in its given form to derive a semi-implicit expression for the eddy-viscosity coefficient C_μ. The development is straightforward. First, the expression is linearized with respect to the mean strain rate, and the definition of the turbulent viscosity (Equations (2) and (3)), with f_μ assumed to be unity, is applied to yield:

$$C_\mu = \frac{(4 - 3C_2)}{\left(6 - 4\eta^2 + 12\zeta^2\right)\left[\left(\frac{C_1}{2} - 1\right) + \frac{P^k}{\varepsilon}\right]}. \tag{13}$$

The production-to-dissipation ratio in the denominator of Equation (13) is expressed by substitution of the following, strictly applicable for incompressible flow:

$$\frac{P^k}{\varepsilon} = \frac{\mu_T S^2}{\rho\varepsilon} = C_\mu \left(\frac{Sk}{\varepsilon}\right)^2. \tag{14}$$

Furthermore, the parameter η^2 can be expressed in terms of Sk/ε, which is the ratio of the strain-rate magnitude to the turbulent time scale. Similarly, ζ^2 can be expressed in terms of Wk/ε, or the ratio of the modified rotation-rate magnitude to the turbulent time scale. After some manipulation to eliminate negative terms on the right-hand-side that could result in a singularity, the following is obtained:

$$C_\mu = \frac{K_1 + K_2 C_\mu \left(\frac{Sk}{\varepsilon}\right)^2 + K_3 C_\mu \left(\frac{Sk}{\varepsilon}\right) + K_4 C_\mu^2 \left(\frac{Sk}{\varepsilon}\right)^3}{K_5 + K_6 C_\mu \left(\frac{Sk}{\varepsilon}\right)^2 + K_7 C_\mu^2 \left(\frac{Sk}{\varepsilon}\right)^4 + K_8 \left(\frac{Wk}{\varepsilon}\right)^2}. \tag{15}$$

While this result for C_μ is not explicit, it is convergent, and may be computed through successive iterations in conjunction with the iterative solution of the dependent variables during the simulation. This is ideally suited for an implicit solver, but it may also be employed in a time-resolved explicit solver by pre-converging C_μ before beginning the time step. A detailed derivation of Equations (13) and (15) is provided in the Appendix.

The influence of reference frame rotation rate, ω_m, on the eddy viscosity occurs via the modified rotation-rate term (Equation (9)). However, two deficiencies with this form are readily apparent. First, the model is clearly not frame indifferent, i.e. the scalar value of C_μ (and therefore μ_T) is arbitrarily dependent on ω_m, since the construction of the modified rotation-rate magnitude, W, is not itself frame indifferent unless $C_4 \to \infty$. Second, the model form does not contain any sensitivity to streamline curvature. These related difficulties may be addressed via two separate considerations. First, the weak equilibrium condition used to arrive at Equation (4) is redefined to correspond to weak equilibrium in a reference frame rotating with the local flow rotation, rather than an arbitrary (or inertial) reference frame. This approach has been adopted by several other authors to yield algebraic Reynolds-stress models that provide improved results in curved and rotating flows (Wallin and Johansson, 2002; Hellsten, 2002; Gatski and Wallin, 2004; Grundestam *et al.*, 2005). Second, the flow rotation rate is defined to correspond to the material (i.e. Lagrangian) rate of rotation of the principal axes of the mean strain-rate tensor, as viewed in an inertial frame of reference. This view of flow rotation was initially proposed by Spalart and Shur (1997). It has the advantage of being Galilean invariant, in contrast to previous models that adopted a definition of flow rotation based on streamline curvature. Another Galilean-invariant definition of flow rotation, proposed by Girimaji (1997), is the material rotation of the acceleration vector. However, it was recently demonstrated that this formulation leads to singularities in the definition of flow rotation and the strain-rate-based form has been shown to be superior (Wallin and Johansson, 2002; Hellsten, 2002).

Since the flow rotation rate, ω_m, depends on the rotation rate of the principal axes of the mean strain-rate tensor, second spatial derivatives of velocity appear in this term and enter the calculation of C_μ via the rotational term W_{ij}. This feature often creates difficulty when used with a complex geometry requiring imperfect (i.e. skewed) structured or unstructured meshes because the explicitly calculated second derivative fields are "noisy" (not smooth), even for a fully converged solution. This is a common trait of numerically approximated higher-order derivatives, and other researchers, such as Shur *et al.* (2000), have discussed the difficulties with using second derivatives in eddy-viscosity models. The present authors have found that it is difficult, if not impossible, to achieve a sensible, converged solution with the above model form where second derivatives appear in the calculation of the eddy viscosity. Unfortunately, it is impossible to remove the higher-order derivatives in the formulation if the exact form of the flow rotation rate is used.

In the eddy-viscosity formulation proposed here, the flow rotation rate is approximated, rather than calculated exactly, in order to eliminate the second derivatives in the calculation of C_μ. It is assumed, for the purpose of approximating the rotation term only, that the local flow conditions correspond to two-dimensional, simple shear flow in a frame rotating with the flow. This turns out to be a reasonable assumption for many engineering flows in which curvature and/or rotation effects are important. In the inertial frame, the rotation-rate tensor in this case can be cast into the simple two-dimensional form:

$$\Omega_{ij} = \begin{bmatrix} 0 & S/2 - \omega_m \\ -S/2 + \omega_m & 0 \end{bmatrix} \tag{16}$$

where the strain-rate magnitude is equal to S in both the rotating and inertial frames and ω_{m} is the flow rotation rate. The fluid rotation-rate magnitude is therefore approximated as

$$\Omega = \sqrt{2\Omega_{ij}\Omega_{ij}} = S - 2\omega_m. \tag{17}$$

The above equation is locally solved for the frame rotation rate, ω_m, which in this case is assumed to be equal to the flow rotation, i.e. the rotation rate of the principle axes of the rate-of-strain tensor:

$$\omega_m = \frac{1}{2}(S - \Omega). \tag{18}$$

For the assumed condition of two-dimensional rotating shear flow, the frame rotation rate may be found exactly with knowledge of the rotation-rate magnitude, Ω, and the strain-rate magnitude, S, both computed in an inertial frame of reference. For the general case of rotating or curved shear flow, Equation (18) represents an approximation of the flow rotation rate. The modified rotation rate tensor W_{ij} may then be calculated in a straightforward manner (see the Appendix for details), and its magnitude W, given below, substituted into the formulation for C_μ.

$$W = \left| S \cdot \left(1 - \frac{C_4 - 4}{C_4 - 2} \right) + \Omega \cdot \left(\frac{C_4 - 4}{C_4 - 2} \right) \right| = \left| \frac{9}{4}\Omega - \frac{5}{4}S \right| \tag{19}$$

The eddy-viscosity formulation described by Equations (15) and (19) is Galilean invariant and frame indifferent, since the eddy viscosity is constructed entirely as a function of the invariant quantities S, Ω, k, and ε.

The remaining model development concerns the valuation of the constants K_1 through K_8 in Equation (15). The rotation-rate constant K_8 was computed using the coefficients in the differential Reynolds-stress model that was used as the starting point for the derivation (Speziale *et al.*, 1991). The remaining constants in Equation (2) were determined by a least-squares best fit to the behavior of C_μ in the realizable k-ε (RKE) model of Shih *et al.* (1995) for the case of zero flow rotation. These constants are given in the Appendix, along with the complete set of model equations. Figure 1 shows the behavior of C_μ as a function of Sk/ε for the zero flow rotation case, and its close reproduction of the RKE behavior.

A two-layer type of near-wall treatment was included in the new turbulence model to allow the integration of the flow to the wall. The model employs the one-equation model of Wolfstein (1969) in the near-wall zone. The transport equation for turbulent kinetic energy is solved within the wall-layer, while the dissipation rate is calculated via an empirical correlation based on local wall distance. There is one new feature of the present wall model, and that is a dynamic scale limiter to avoid the turbulent Reynolds number cutoff (usually$Re_y = \sqrt{k} \cdot y/\nu = 200$) commonly employed to differentiate between near-wall and far-field (i.e. high-Re) zones. In the present model, during each iteration, length scales are calculated at each cell based on the "high-Reynolds number" model and the near-wall model, and the minimum of the two values is used. This allows the size of the near-wall zone to simply adjust to the local flow conditions, and it eliminates the need to define an *ad hoc* wall distance cutoff for the two-layer model. To validate the near-wall model, simulations of fully developed channel flow were conducted at several Reynolds numbers. The boundary layer profile in wall units for $Re_\tau = 395$ is shown in Figure 2, and good agreement is observed with data from the DNSs of Kim *et al.* (1987).

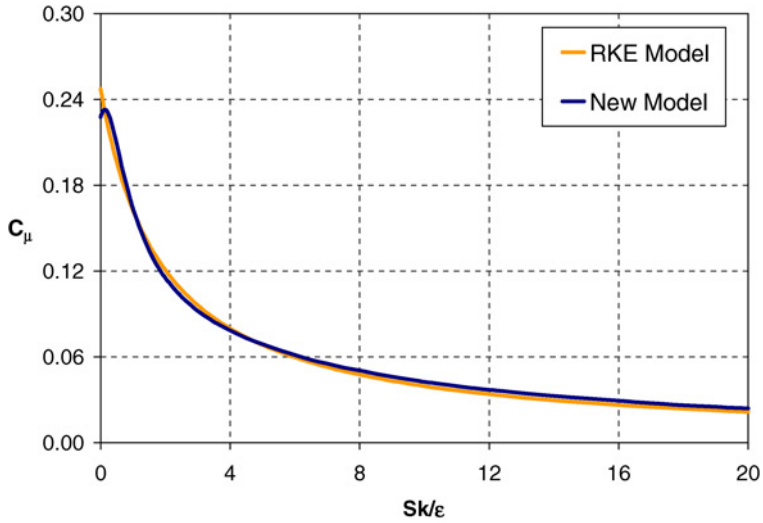

Note: The variable coefficient closely matches that of the realizable k-ε (RKE) model of Shih *et al.* (1995)

Figure 1.
Eddy-viscosity coefficient, C_μ, plotted as a function of the mean-to-turbulent time scale ratio, Sk/ε, for non-rotating shear flow

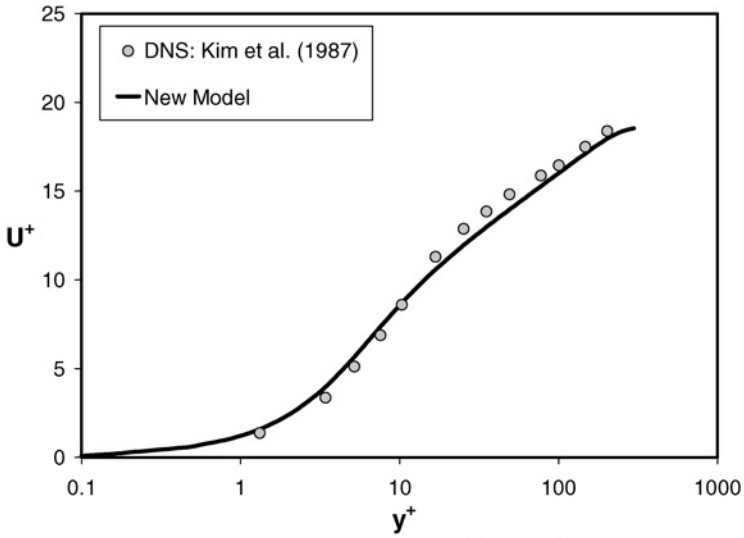

Note: The new model shows good agreement with DNS data

Figure 2.
Prediction of velocity profile in fully developed, non-rotating channel flow at $Re_\tau = 395$ using the new turbulence model with dynamic two-layer near-wall treatment

Simulation details

The new curvature-sensitive eddy-viscosity model was implemented into fluent version 6.1.22 software via user-defined function (UDF) capability. For comparison, simulations of the test cases were also conducted with the standard k-ε (SKE) model (Launder and Spalding, 1972) and the RKE model (Shih *et al.*, 1995), with two-layer near-wall modeling. Simulations were run using the SIMPLE pressure-correction solver, and a second-order upwind convective discretization scheme for all flow variables. For the turbine vane conjugate heat transfer simulation, the Fourier equation for heat diffusion was solved in the solid zone, and fluid–solid heat transfer coupling was accomplished by enforcing conservation of the heat flux at the fluid–solid interface.

Convergence of all solutions was verified with the following strict criteria:

- residuals of the governing equations, normalized by their respective inlet fluxes, fell below 0.1 percent;
- global mass and energy imbalances dropped below 0.01 percent; and
- the flow field was unchanging, based on observation of profiles of velocity, pressure, temperature and turbulence quantities.

Additionally, solution-based grid adaption was used to refine the mesh and obtain a new converged solution. This process was repeated until the solution was unchanging, and grid-independence was declared.

The two-dimensional simulations (rotating channel and U-bend) were run on a single processor of a SunBlade 2000 computer. The three-dimensional turbine vane conjugate heat transfer case had a mesh of 6.7 million finite volumes, and these simulations were run on 20 parallel processors of a Sun Enterprise 6500 machine. The new turbulence model took no more than 5 percent more time per iteration than the SKE and RKE models, and the number of iterations required for convergence was approximately equal between all models.

Test cases

This section discusses a series of test cases intended to gauge the performance of the new model, both in an absolute sense by comparison of simulation results to data from experiment or DNS, and in a relative sense through comparison with the standard k-ε and realizable k-ε model results. All of the cases exhibit flow development and/or heat transfer that is strongly dependent on curvature or rotation. The first case is simple rotating homogenous shear flow, in order to demonstrate the response of the model to stabilizing or destabilizing rotation. The next two cases are two-dimensional problems – fully developed flow in a rotating channel and channel "U-bend" flow. The fourth test case is a conjugate heat transfer simulation of an internally cooled gas turbine vane. This case is intended to highlight the effectiveness of the new model in a realistic application problem that might be encountered in a design environment, as well as model robustness for use with a complex problem requiring a large, unstructured grid.

Rotating homogeneous shear flow

Homogeneous shear flow is a well-studied and understood demonstration case for the effect of rotation on turbulence production mechanisms. Figure 3 shows the temporal evolution of turbulent kinetic energy for the non-rotating case ($\omega_m/S = 0$), indicating good agreement between the new model and the reference LES results (Bardina *et al.*, 1983). In comparison, the standard k-ε model indicates a more energetic response, as shown. Figure 4 shows the effect of stabilizing rotation ($\omega_m/S = -0.5$). Despite the applied mean shear, the turbulent kinetic energy undergoes a monotonic decay. This behavior is well predicted by the new model, while the SKE model, which is insensitive to rotation and curvature, shows identical behavior as the zero-rotation case. Lastly, Figure 5 shows the effect of destabilizing rotation ($\omega_m/S = 0.25$), which increases the growth rate of turbulent kinetic energy relative to the zero rotation case. Boussinesq-based models assume instantaneous response of the turbulence structure to changes in mean strain rate, so the initial time lag between application of mean strain and

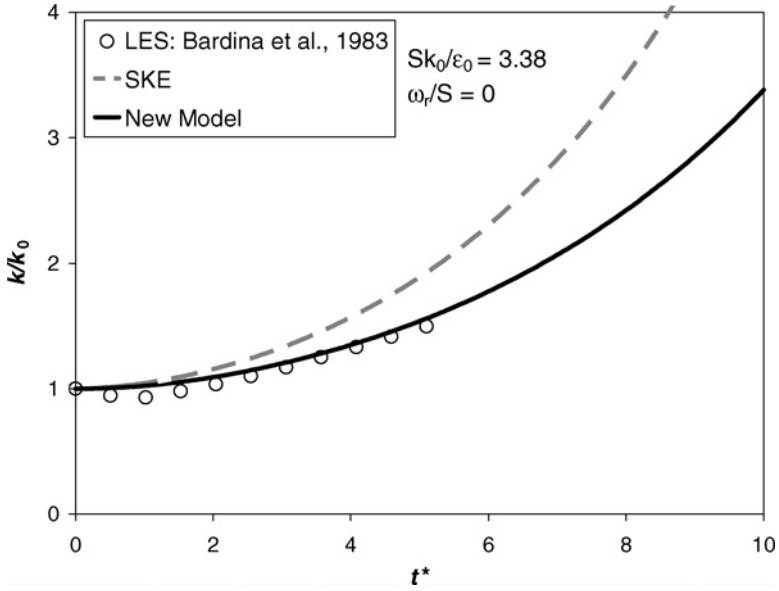

Figure 3.
Temporal growth of turbulent kinetic energy for non-rotating homogeneous turbulence in plane shear

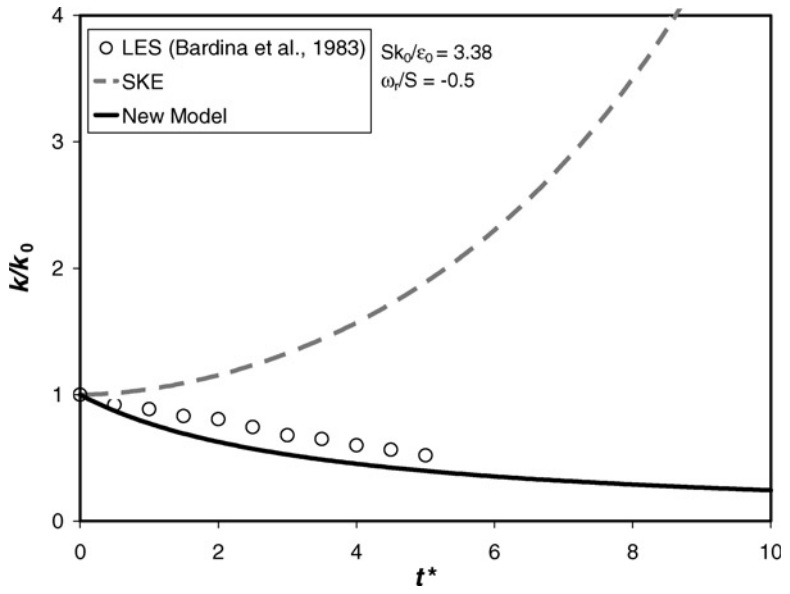

Figure 4.
Temporal growth of turbulent kinetic energy for homogeneous turbulence under plane shear with stabilizing rotation

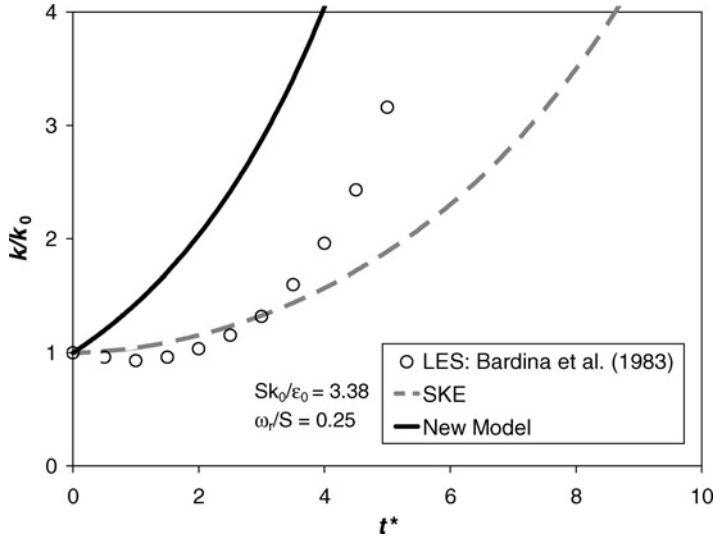

Figure 5.
Temporal growth of turbulent kinetic energy for homogeneous turbulence under plane shear with destabilizing rotation

turbulence growth apparent in the LES results is not reproduced by either of the eddy-viscosity models. However, the new model shows an overall similar behavior to the LES results, indicating that the new eddy-viscosity formulation yields the correct response to both stabilizing and destabilizing rotation, as expected.

Rotating channel flow

The fairly simple test case of two-dimensional, fully developed rotating channel flow isolates the effects of flow rotation on the wall-bounded turbulence field. A schematic of

the problem setup is shown in Figure 6. In order to match the conditions of the DNS by Kristoffersen and Andersson (1993), the Reynolds number based on the wall friction velocity and the channel half height ($H/2$) was fixed at $\mathrm{Re}_\tau = 194$. Simulations were conducted for Rotation numbers $\mathrm{Ro} = \frac{\omega_m H}{U_m} = 0$ (non-rotating reference case), $\mathrm{Ro} = 0.05$, and $\mathrm{Ro} = 0.5$. In addition to the new model, the standard k-ε model was employed for comparison purposes.

Velocity profiles for the reference case with zero rotation are shown in Figure 7. The new model shows excellent agreement with the symmetric DNS profile, slightly better than the SKE model. This implies that the new near-wall treatment is physically appropriate, since much of the channel lies in the near-wall (one-equation) zone at this low Reynolds number. Because the flow is fully developed with no transverse component of velocity, there is no effect of system rotation directly on the mean flow. In fact, laminar, fully developed flow will maintain a symmetric profile regardless of any imposed rotation. The turbulence is, however, affected by rotation, and any asymmetry in the turbulence across the channel will result in skewness in the mean velocity profile.

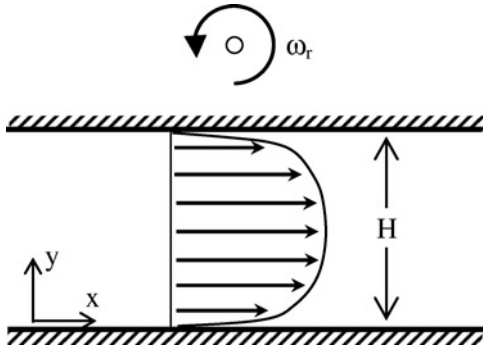

Figure 6.
Diagram of rotating, fully developed, turbulent channel flow problem

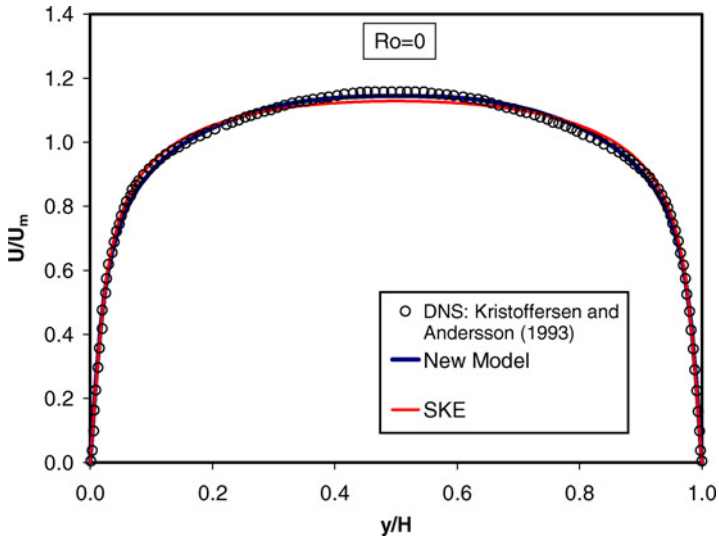

Figure 7.
Velocity profiles for non-rotating (Ro = 0) turbulent channel flow reference case

Figures 8 and 9 show the velocity and turbulent kinetic energy profiles, respectively, for a mild rotation rate of Ro = 0.05. The turbulent kinetic energy is normalized as $k^+ = \frac{k}{u*^2}$. The DNS data show that the velocity and turbulent kinetic energy profiles have become skewed due to the effects of rotation on the turbulence. The new model correctly predicts the skewed velocity profile. The SKE model does not, which is not surprising since the model has no sensitivity to the flow rotation. The new model shows asymmetry in the turbulent kinetic energy, with reduced k near the suction

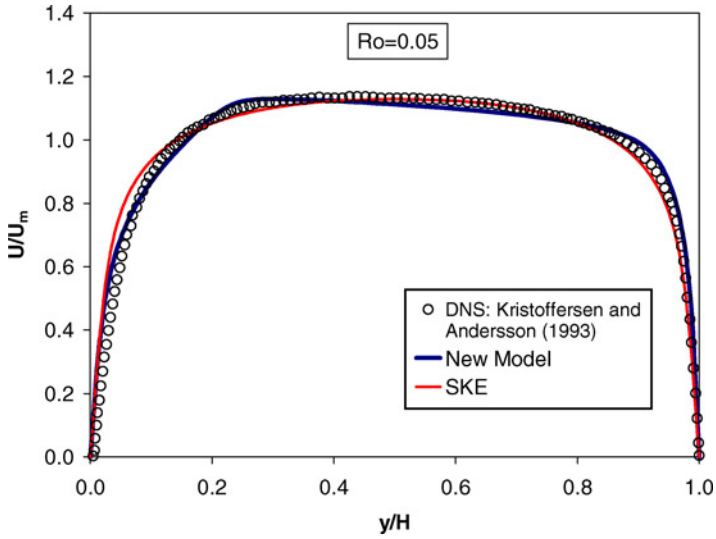

Figure 8.
Velocity profiles for channel flow at a mild rotation rate of Ro = 0.05 showing skewness accurately predicted by the new model

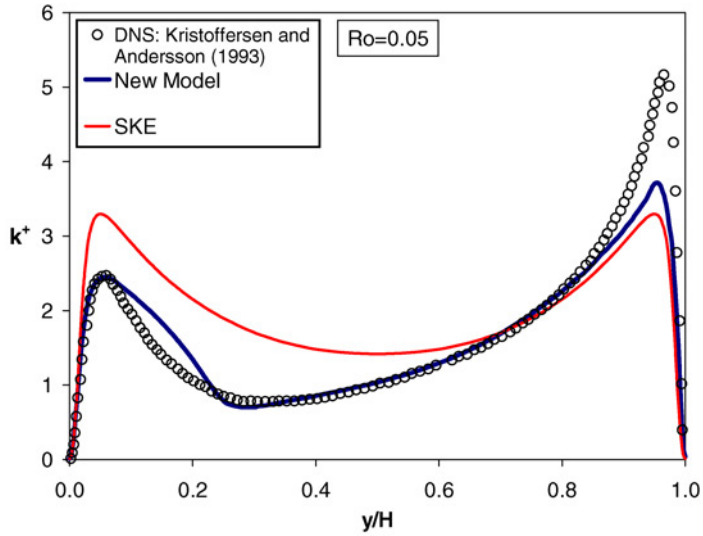

Figure 9.
Turbulent kinetic energy profiles for rotating channel flow with Ro = 0.05

Note: The SKE model shows no sensitivity to the rotation

surface ($y/H = 0$) and augmented k near the pressure surface ($y/H = 1$), although the turbulence level here is slightly underpredicted.

As the rotation is increased to a relatively large level of Ro = 0.5, the profiles for velocity and turbulent kinetic energy, shown in Figures 10 and 11, display strong asymmetry. The new model results show excellent agreement with the DNS velocity profile. Qualitatively, the new model captures the skewness in the turbulent kinetic energy profile, although k is underpredicted near the suction surface and slightly overpredicted near the suction surface. For this case, it is again apparent that the SKE is completely insensitive to rotation.

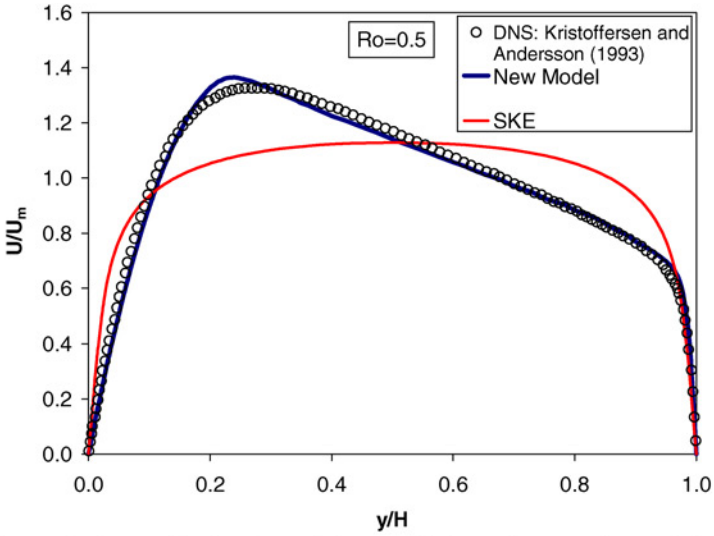

Note: Velocity profiles for channel flow at a high rotation rate of Ro = 0.5 clearly show the sensitivity of the new model to rotation and the lack of response of SKE

Figure 10.

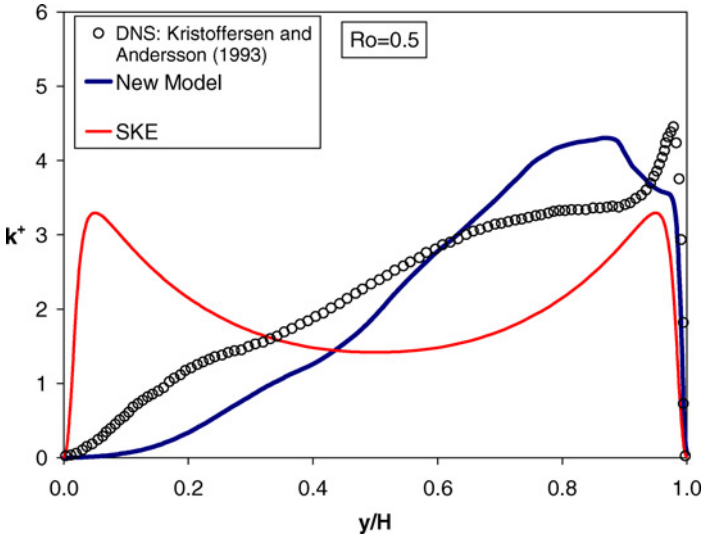

Figure 11.
Turbulent kinetic energy profiles for channel flow with rotation number Ro = 0.5

U-bend flow

The problem of flow in a U-bend, or 180° turnaround duct, is designed to highlight the model performance when streamlines are strongly curved. The U-bend simulations match the experimental geometry and conditions of Monson *et al.* (1990). The radius of the turn (at the channel centerline) is equal to the channel height, H. The computational domain is shown in Figure 12. The Reynolds number based on the mean velocity and the channel height was $\mathrm{Re}_H = 10^6$. Inlet conditions in the numerical simulations were prescribed to match the experimental profiles for mean streamwise velocity and turbulent kinetic energy at $s/H = 0$, and these profiles are shown in Figure 13. Note that y is the wall-normal direction and is always measured from the inside surface to the outside surface. In addition to the new model, results were obtained for the SKE and RKE models.

Figure 14 shows flow development in the bend section at $\theta = 90^o$ (halfway through the bend) in terms of the streamwise velocity and the turbulent kinetic energy profiles, both normalized by the average velocity across the channel. Observing the profiles for turbulent kinetic energy first, the experiments show a significant increase in k near the outer surface ($y/H = 1$) and a decrease in k near the inner surface ($y/H = 0$). This is because the concave curvature has a destabilizing effect on turbulence, while the convex curvature has a stabilizing effect. The behavior in response to the streamline curvature along the outer and inner walls is analogous to the response on the pressure and suction surfaces, respectively, for the rotating channel case discussed above. The SKE model shows no sensitivity to the curvature, with a nearly symmetric profile for k, while the

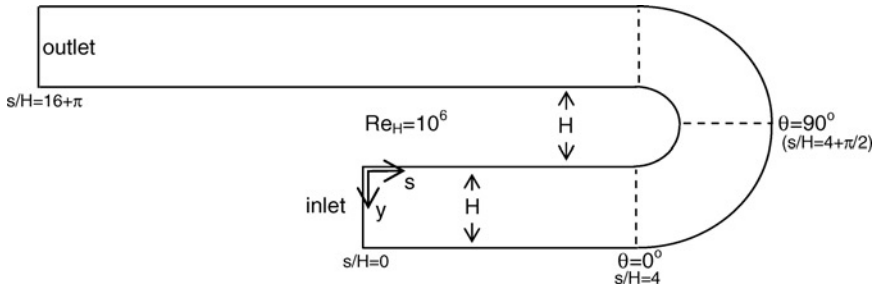

Figure 12.
Computational domain for two-dimensional U-bend simulation

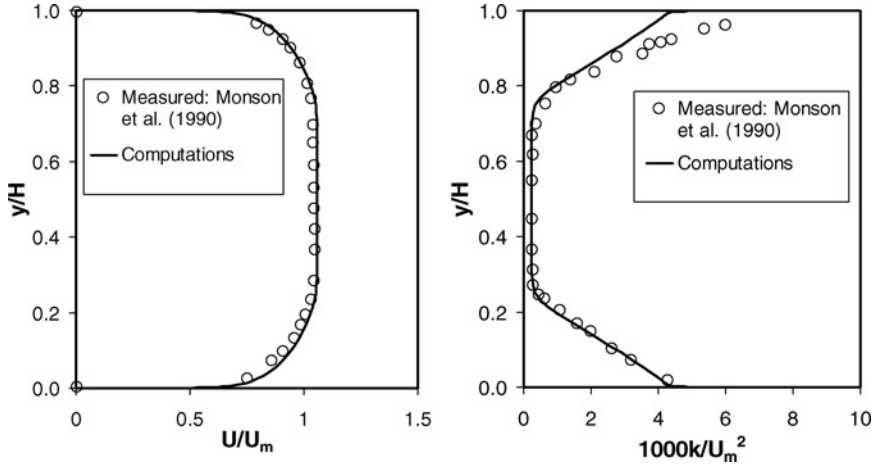

Figure 13.
Profiles of normalized velocity and turbulent kinetic energy at the inlet of the computational domain indicating a good match of the experimental conditions

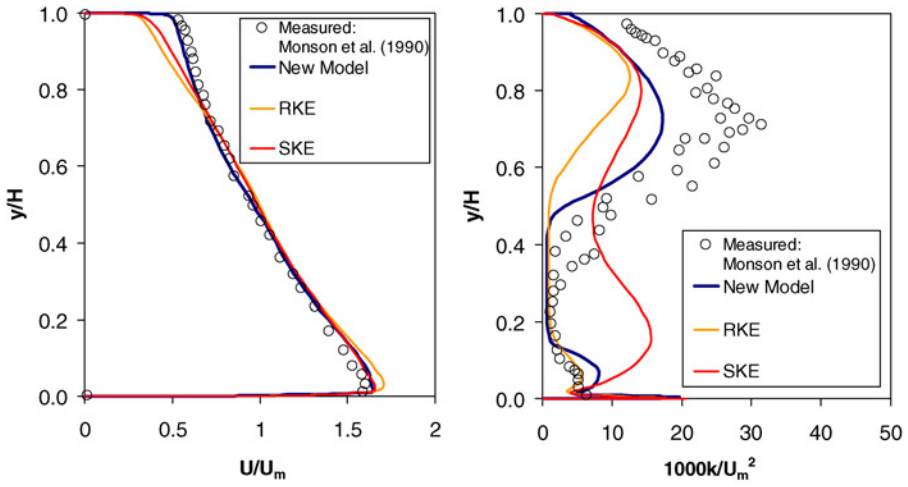

Note: Profiles of velocity and turbulent kinetic energy at $\theta = 90^{\circ}$ in the U-bend show that the new model is better able to capture augmented turbulence near the outer surface and its effect on the mean velocity

Figure 14.

RKE model shows only a slight response. Only the new model qualitatively predicts the profile for k, correctly matching the shape and location of the peak near the outer surface. The elevated turbulence has an impact on the mean flow near the outside wall, and only the new model predicts a full profile for U that matches the measured data.

Figure 15 shows the profiles for normalized U and k at $\theta = 180^{o}$, the exit to the U-bend section. Experiments indicate a flow separation zone, with a negative streamwise velocity component, near the inside surface. The SKE model predicts excess turbulence near $y/H = 0$, despite the natural tendency of the convex curvature to reduce k. Because of the excess momentum transport due to artificially high levels of k here, SKE indicates almost no separation at all. The RKE model shows a very slight separation. The new model correctly predicts separation and is closest to the measured values. A large peak in

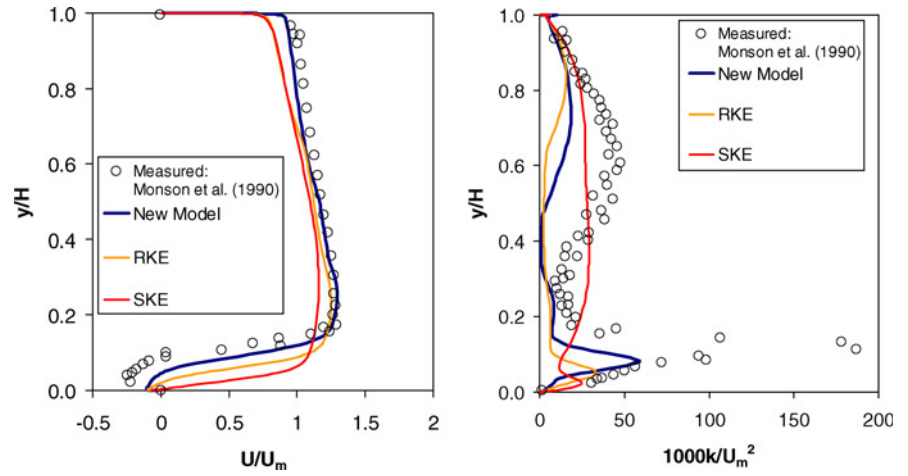

Figure 15.
Profiles of velocity and turbulent kinetic energy at $\theta = 180^{o}$ (end of U-bend section)

k near the inside wall corresponds to the location of the shear layer between the recirculation zone and the high-speed flow above it. The new model alone predicts the location of the peak, although all models underpredict the magnitude. It is believed that this is largely due to the presence of unsteady effects in the experiment that are not resolved in the steady-state measurements, a mechanism not studied herein.

In Figures 16 and 17, predictions are presented for the skin friction coefficient for the inner and outer walls, respectively. The location of the curved section is between $s/H = 4$ and $s/H = (4 + \pi)$, denoted by the dashed lines in the plots. The new model indicates a lower value for C_f on the inner wall in the bend, and this is in better agreement with the experiment than the other two models. This is an effect of the new

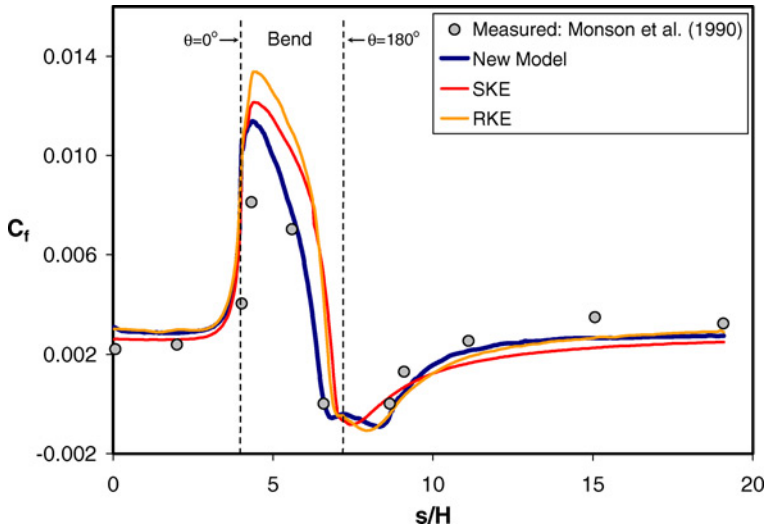

Figure 16.
Distribution of the skin friction coefficient on inner wall of the U-bend

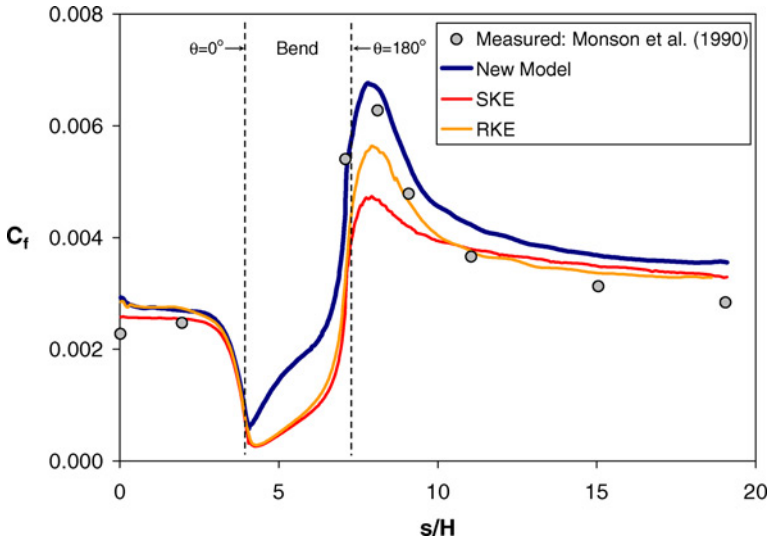

Figure 17.
Distribution of the skin friction coefficient on outer wall of the U-bend

model correctly predicting a decrease in turbulence along the inner, convex wall, which tends to reduce the wall shear stress. The opposite trend should be seen on the outer, or concave, wall, and indeed the new model predicts a higher skin friction in and after the bend, which is in line with the measurements. The new model does slightly overpredict the friction well downstream of the bend (beyond $s/H = 10$), however this is believed to be primarily a function of separation zone behavior and not an indicator of the model's curvature sensitivity.

Turbine vane conjugate heat transfer

A conjugate heat transfer simulation of an internally cooled gas turbine vane at engine-realistic conditions was conducted to provide a complex, realistic problem on which to test the robustness of new turbulence model. The conjugate approach involves a single simulation in which the heat transfer modes (external convection, diffusion in the solid and internal convection) are fully coupled. York and Leylek (2003) provide further discussion of the conjugate heat transfer approach and the gas turbine vane simulation. It is expected that curvature effects on the turbulence (and therefore heat transfer) are important, especially on the suction surface with its strong convex curvature. Matching the experimental conditions of Hylton *et al.* (1983), the geometry was a "C3X" vane, made of stainless steel 310, in a linear cascade arrangement. A combustor supplied hot air at $T_o = 796$ K for the main flow, and the vane was cooled by air at $T_c = 300$ K flowing radially through ten round channels in the part. A view of the computational domain is given in Figure 18. The Reynolds number based on true chord and conditions at the trailing edge plane was $\mathrm{Re}_c = 1.9 \times 10^6$. The maximum Mach number in the vane passage was approximately 0.9. In the numerical simulation, fluid properties and the vane thermal conductivity were taken to be second-order polynomial functions of temperature. A view of the computational mesh on the midspan plane is shown in Figure 19.

Figure 20 shows contours of the turbulence level (defined based on the average velocity at the inlet) on the midspan plane near the very strong curvature of the suction surface for the RKE model and the new model. Very near the wall, the RKE model predicts turbulence levels in the freestream in excess of 30 percent. This response reflects the so-called "stagnation point anomaly" in which eddy-viscosity turbulence models show an overprediction of turbulence in rapidly strained regions of the freestream flow (Durbin, 1996). Through the modified eddy-viscosity coefficient, the new model responds to the irrotational strain rate in a more realistic manner, indicating that the freestream turbulence production is minimal, and the majority of turbulence production predicted to be within the boundary layer. While not clearly visible in the contours, the new model also predicts decreased levels of turbulence in the boundary layer that is developing on the convex airfoil surface. It is expected that the stabilizing effect of convex curvature should decrease the heat transfer coefficient in this region. Indeed this is the case, as seen in Figure 21, showing predicted Stanton number (based on average conditions at the trailing edge plane) distributions at midspan for the two turbulence models. Because the new model was calibrated to behave as a realizable k-ε when no flow rotation (curvature) is present, it should be no surprise that predicted Stanton number is comparable everywhere except the strong convex curvature portion of the suction surface. The new model does predict a small increase in heat transfer, a result of turbulence augmentation, on the leading two-thirds of the pressure surface, which is characterized by mild concave curvature.

The predictions of normalized static temperature (θ) distribution on the vane external surface at the midspan are plotted in Figure 22, along with the measured data of Hylton *et al.* (1983). This temperature depends directly on the local heat transfer

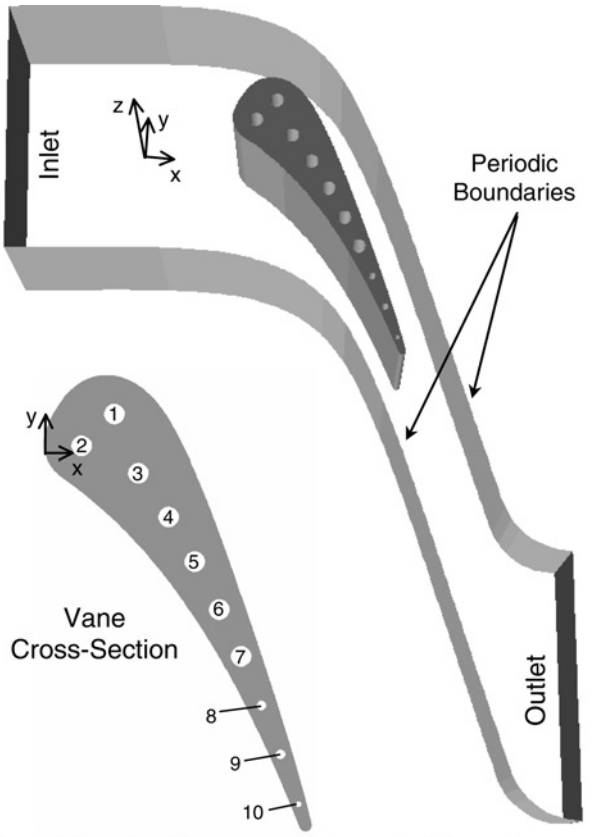

Figure 18.
Diagram of the computational domain with a cross-sectional view of the vane

Note: Note that the transparent (spanwise) boundaries are solid walls

coefficient. The SKE model results are included in this plot, and the predictions with this model are significantly higher than the measurements over the entire surface. York and Leylek (2003) explained that this is primarily due to the spurious production of turbulent kinetic energy near the airfoil leading edge and in the passage exhibited by the standard model. The RKE model produces reasonably good results for wall temperature over the vane surface, with the exception of the strong curvature portion of the suction surface. The overprediction in temperature by the RKE model corresponds to the location of the peak in the Stanton number on the suction surface. The new curvature-corrected model addresses this shortcoming of the other k-ε models. Due to lower predicted heat transfer coefficients on the suction surface where convex curvature is the strongest (near $s/L_{ss} = 0.2$), the surface temperature curve with the new model falls close to the level of the experimental data in this region.

Summary and conclusions

This paper presents a new eddy-viscosity formulation that was developed to include appropriate sensitivity to streamline curvature and rotation effects in linear two-equation turbulence models. The influence of rotation and curvature has been included based on invariance arguments and physical interpretation of the influence of flow

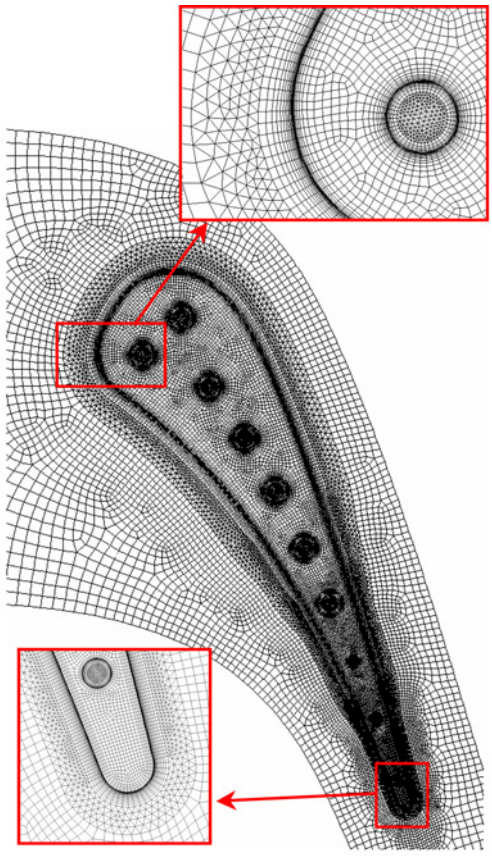

Note: The 3-D mesh contains approximately 6.7 million finite volumes

Figure 19.
View of the computational mesh for the C3X turbine vane conjugate heat transfer simulation

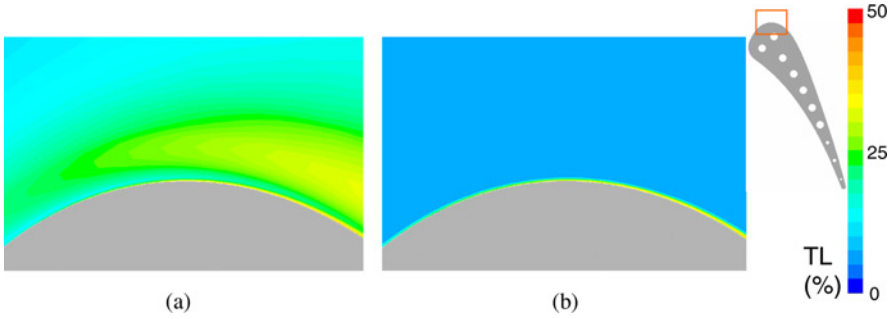

Figure 20.
Contours of turbulence level (based on inlet velocity) near the suction surface on the midspan plane of the C3X vane conjugate heat transfer simulation using (a) RKE model and (b) the new model

rotation rate on turbulence production. The eddy-viscosity model was designed for economic, effective use on any complex flow problem and with unstructured, multi-topology meshes. To this end, second derivatives of the velocity field were eliminated in the flow rotation numerical definition. The exact calculation of local flow rotation has been replaced with an approximation expressed solely in terms of the strain-rate

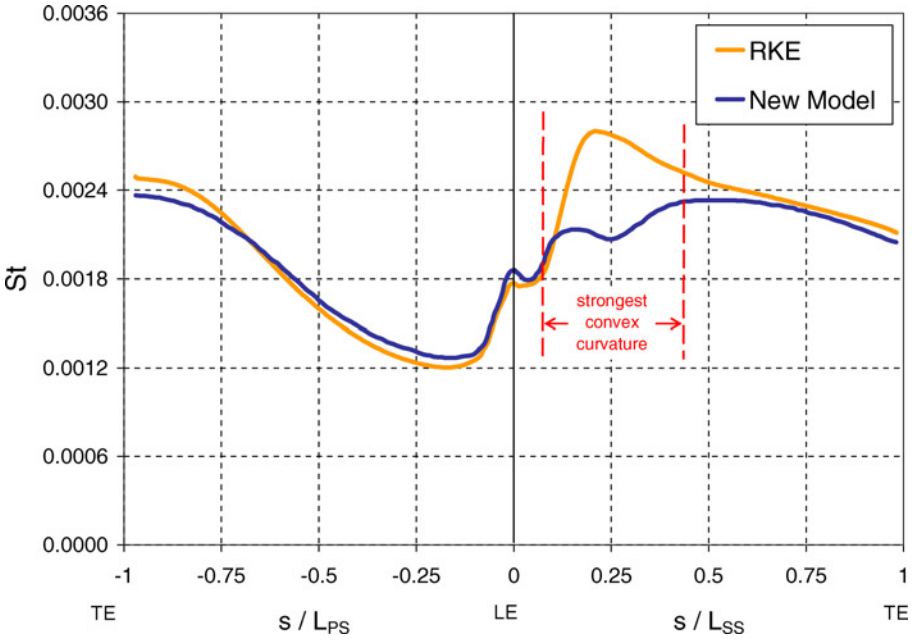

Figure 21.
Stanton number distribution on the C3X vane at the midspan predicted by the RKE model and the new model

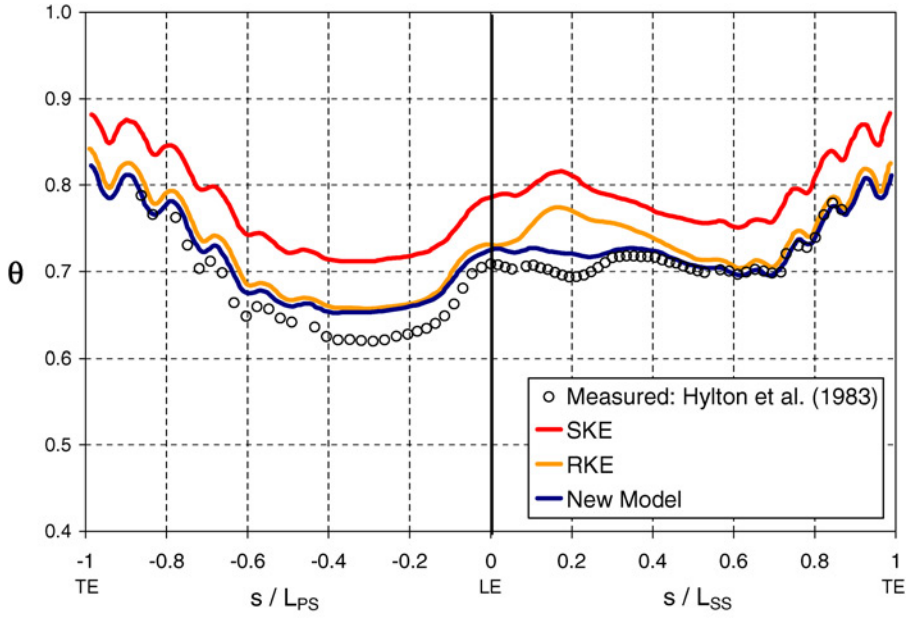

Figure 22.
Vane external surface temperature (normalized) at midspan for the conjugate heat transfer turbine vane simulation

Note: The new model improves predictions significantly on the suction surface, where strong convex curvature exists

magnitude and the rotation-rate magnitude obtained in an inertial frame of reference. The resulting formulation for eddy viscosity is simple and robust, and satisfies principles of frame invariance and realizability.

The new eddy-viscosity formulation was implemented into a standard k-ε model form. A robust two-layer type of near-wall model with dynamic length scale limiting was included for integration to the wall, although the high-Reynolds number model form can also be used in conjunction with a wall-function approach, or damping functions may be used in low-Re versions of either k-ε or k-ω models.

The new turbulence model was tested on several problems for which measured or DNS data were available for validation, and results were also compared to the standard k-ε and realizable k-ε models. For rotating homogeneous turbulence, the new model showed the appropriate attenuation and augmentation of turbulence production for the cases of stabilizing and destabilizing rotation, respectively. For fully developed channel flow, the new model gave excellent predictions for the velocity profiles across the channel, which become more skewed as the rotational speed increases, and qualitatively correct trends in the turbulent kinetic energy predictions. For two-dimensional flow in a U-bend, the new model exhibited the correct response to the curvature, with turbulence augmentation on the concave wall and attenuation on the convex wall. Predictions with the new model for both velocity and turbulence profiles in the bend were much closer than those measured with the SKE or RKE models. Finally, a three-dimensional gas turbine vane aerothermal problem was intended to serve as a stringent, industry-relevant test case with complex geometry and a large, multi-topology mesh. The new model showed reduced levels of turbulence near the vane suction surface where convex curvature was strongest as compared to the RKE model. This resulted in lower heat transfer coefficients and surface temperature in this region, which were in much better agreement with the measured values.

Results for all of the test cases indicate the new model shows a qualitatively correct response to flow rotation and streamline curvature. Due to its simplicity, it is expected that the new model can offer a useful alternative to more complex modeling approaches (differential and algebraic Reynolds-stress models, non-linear two-equation models), particularly since the new eddy-viscosity formulation can be implemented as a "plug-in" to existing linear eddy-viscosity models. Retaining the economy of k-ε variant models and exhibiting efficient, trouble-free convergence for problems of varying complexity, the new eddy-viscosity model offers promise as a robust and efficient tool for use in a design environment.

References

Abid, R., Morrison, J.H., Gatski, T.B. and Speziale, C.G. (1996), "Prediction of aerodynamic flows with a new explicit algebraic stress model", *AIAA Journal*, Vol. 34, pp. 2632-5.

Bardina, J., Ferziger, J.H. and Reynolds, W.C. (1983), "Improved turbulence models based on large-eddy simulation of homogeneous, incompressible turbulent flows", Stanford University Technical Report, TF-19, Stanford, CA.

Bradshaw, P. (1973), "The effects of streamline curvature on turbulent flow", *AGARDograph No. 169*.

Durbin, P. (1996), "On the k-ε stagnation point anomaly", *International Journal of Heat and Fluid Flow*, Vol. 17, pp. 89-90.

Durbin, P.A. (1991), "Near-wall turbulence closure modeling without 'damping functions'", *Theoretical and Computational Fluid Dynamics*, Vol. 3, pp. 1-13.

Fu, S. and Qian, W.Q. (2002), "Development of a curvature sensitive nonlinear eddy-viscosity model", *AIAA Journal*, Vol. 40 No. 11, pp. 2225-33.

Gatski, T.B. and Speziale, C.G. (1993), "On explicit algebraic stress models for complex turbulent flows", *Journal of Fluid Mechanics*, Vol. 254, pp. 59-78.

Gatski, T.B. and Wallin, S. (2004), "Extending the weak-equilibrium condition for algebraic Reynolds stress models to rotating and curved flows", *Journal of Fluid Mechanics*, Vol. 518, pp. 147-55.

Girimaji, S.S. (1997), "A Galilean invariant explicit algebraic Reynolds stress model for turbulent curved flows", *Physics of Fluids*, Vol. 9, pp. 1067-77.

Gooray, A.M., Watkins, C.B. and Aung, W. (1985), "Improvements to the k-ε model for prediction of turbulent recirculating flows", *Proceedings of the Fifth Symposium on Turbulent Shear Flows*, *Cornell University, Ithaca, NY*, pp. 18.26-18.31.

Grundestam, O., Wallin, S. and Johansson, A.V. (2005), "An explicit algebraic Reynolds stress model based on a nonlinear pressure strain rate model", *International Journal of Heat and Fluid Flow*, Vol. 26, pp. 732-45.

Hellsten, A. (2002), "Curvature corrections for algebraic Reynolds stress modeling: a discussion", *AIAA Journal*, Vol. 40, pp. 1909-11.

Hoffman, P.H., Muck, K.C. and Bradshaw, P. (1985), "The effect of concave surface curvature on turbulent boundary layers", *Journal of Fluid Mechanics*, Vol. 161, pp. 371-403.

Howard, J.H.G., Patankar, S.V. and Bordynuik, R.M. (1980), "Flow prediction in rotating ducts using Coriolis-modified turbulence models", *ASME Journal of Fluids Engineering*, Vol. 102, pp. 456-61.

Hylton, L.D., Milhec, M.S., Turner, E.R., Nealy, D.A. and York, R.E. (1983), "Analytical and experimental evaluation of the heat transfer distribution over the surface of turbine vanes", *NASA CR 168015*.

Iacovides, H., Launder, B.E. and Li, H.-Y. (1996), "The computation of flow development through stationary and rotating U-ducts of strong curvature", *International Journal of Heat and Fluid Flow*, Vol. 17, pp. 22-33.

Kim, J., Moin, P. and Moser, R.D. (1987), "Turbulence statistics in fully-developed channel flow at low Reynolds number", *Journal of Fluid Mechanics*, Vol. 177, pp. 133-86.

Kristoffersen, R. and Andersson, H.I. (1993), "Direct numerical simulation of low Reynolds-number turbulent flow in a rotating channel", *Journal of Fluid Mechanics*, Vol. 256, pp. 163-97.

Launder, B.E. and Spalding, D.B. (1972), *Lectures in Mathematical Models of Turbulence*, Academic Press, London.

Launder, B.E., Priddin, C.H. and Sharma, B.I. (1977), "The calculation of turbulent boundary layers on spinning and curved surfaces", *ASME Journal of Fluids Engineering*, Vol. 99, pp. 231-9.

Leschziner, M.A. and Rodi, W. (1981), "Calculation of annular and twin parallel jets using various discretization schemes and turbulence-model variations", *ASME Journal of Fluids Engineering*, Vol. 103, pp. 352-60.

Monson, D.J., Seegmiller, H.L., McConnaughey, P.K. and Chen, Y.S. (1990), "Comparison of experiment with calculations using curvature-corrected zero and two equation turbulence models for a two-dimensional U-duct", *AIAA*, Paper No. 90-1484.

Muck, K.C., Hoffman, P.H. and Bradshaw, P. (1985), "The effect of convex surface curvature on turbulent boundary layers", *Journal of Fluid Mechanics*, Vol. 161, pp. 347-69.

Park, S.W. and Chung, M.K. (1989), "Curvature-dependent two-equation model for prediction of turbulent recirculating flows", *AIAA Journal*, Vol. 27, pp. 340-4.

Pettersson Reif, B.A., Durbin, P.A. and Ooi, A. (1999), "Modeling rotational effects in eddy viscosity closures", *International Journal of Heat and Fluid Flow*, Vol. 20, pp. 563-73.

Rumsey, L.R. and Gatski, T.B. (2001), "Isolating curvature effects in computing wall-bounded turbulent flows", *AIAA*, Paper No. 2001-0725.

Shih, T.-H., Liou, W.W., Shabbir, A. and Zhu, J. (1995), "A new k-ε eddy-viscosity model for high Reynolds number turbulent flows: model development and validation", *Computers and Fluids*, Vol. 24 No. 3, pp. 227-38.

Shur, M.L., Strelets, M.K., Travin, A.K. and Spalart, P.R. (2000), "Turbulence modeling in rotating and curved channels: assessing the Spalart–Shur correction", *AIAA Journal*, Vol. 38, pp. 784-92.

Song, B., Amano, R.S. and Liu, G.R. (2001), "On computations of complex turbulent flow by using a nonlinear k-ω model", *Numerical Heat Transfer, Part B*, Vol. 39, pp. 421-34.

Spalart, P.R. and Allmaras, S.R. (1992), "A one-equation turbulence model for aerodynamic flows", *AIAA*, Paper No. 92-0439.

Spalart, P.R. and Shur, M.L. (1997), "On the sensitization of turbulence models to rotation and curvature", *Aerospace Science and Technology*, Vol. 1 No. 5, pp. 297-302.

Speziale, C.G. and Mac Giolla Mhuiris, N. (1989), "On the prediction of equilibrium states in homogeneous turbulence", *Journal of Fluid Mechanics*, Vol. 209, pp. 591-615.

Speziale, C.G., Sarkar, S. and Gatski, T.B. (1991), "Modelling the pressure-strain correlation of turbulence: an invariant dynamical systems approach", *Journal of Fluid Mechanics*, Vol. 227, pp. 245-72.

Wallin, S. and Johansson, A.V. (2002), "Modelling streamline curvature effects in explicit algebraic Reynolds stress turbulence models", *International Journal of Heat and Fluid Flow*, Vol. 23, pp. 721-30.

Wang, X. and Thangam, S. (2006), "Development and application of an anisotropic two-equation model for flows with swirl and curvature", *ASME Journal of Applied Mechanics*, Vol. 73, pp. 397-404.

Wilcox, D.C. (1988), "Reassessment of the scale-determining equation for advanced turbulence models", *AIAA Journal*, Vol. 26, pp. 1299-310.

Wolfstein, M. (1969), "The velocity and temperature distribution of one-dimensional flow with turbulence augmentation and pressure gradient", *International Journal of Heat and Mass Transfer*, Vol. 12, pp. 301-18.

Yang, X. and Ma, H. (2003), "Computation of strongly swirling confined flows with cubic eddy-viscosity turbulence models", *International Journal for Numerical Methods in Fluids*, Vol. 43, pp. 1355-70.

York, W.D. and Leylek, J.H. (2003), "Three-dimensional conjugate heat transfer simulation of an internally-cooled gas turbine vane", *ASME,* Paper No. GT2003-38551.

Appendix: New model equations

The equations for the new curvature-sensitive turbulence model are listed below in their generalized, compressible form. The model is a two-equation k-ε model, and the curvature/rotation effects enter through the algebraic expression for the eddy-viscosity. The eddy-viscosity formulation is also designed to satisfy the realizability constraint for the turbulent stresses. The "high-Reynolds number" model form is coupled with a dynamic two-layer near-wall model for integration down to the wall.

Turbulent kinetic energy transport equation

$$\frac{\partial(\bar{\rho}k)}{\partial t}+\frac{\partial}{\partial x_j}\left(\bar{\rho}U_j k\right)=\frac{\partial}{\partial x_j}\left[\left(\mu+\frac{\mu_T}{Pr_k}\right)\frac{\partial k}{\partial x_j}\right] + \left[2\mu_T\left(S_{ij}-\frac{1}{3}\delta_{ij}\frac{\partial U_k}{\partial x_k}\right)-\frac{2}{3}\bar{\rho}k\delta_{ij}\right]\frac{\partial U_i}{\partial x_j}-\bar{\rho}\varepsilon \tag{A.1}$$

Turbulence dissipation rate transport equation

$$\frac{\partial(\bar{\rho}\varepsilon)}{\partial t}+\frac{\partial}{\partial x_j}\left(\bar{\rho}U_j\varepsilon\right)=\frac{\partial}{\partial x_j}\left[\left(\mu+\frac{\mu_T}{Pr_\varepsilon}\right)\frac{\partial\varepsilon}{\partial x_j}\right] + C_{\varepsilon 1}\frac{\varepsilon}{k}\left[2\mu_T\left(S_{ij}-\frac{1}{3}\delta_{ij}\frac{\partial U_k}{\partial x_k}\right)-\frac{2}{3}\bar{\rho}k\delta_{ij}\right]\frac{\partial U_i}{\partial x_j}-C_{\varepsilon 2}\bar{\rho}\frac{\varepsilon^2}{k} \tag{A.2}$$

Turbulent viscosity definition

$$\mu_T=C_\mu\bar{\rho}\frac{k^2}{\varepsilon} \tag{A.3}$$

Turbulent viscosity coefficient

$$C_\mu=\frac{K_1+K_2C_\mu\left(\frac{Sk}{\varepsilon}\right)^2+K_3C_\mu\left(\frac{Sk}{\varepsilon}\right)+K_4C_\mu^2\left(\frac{Sk}{\varepsilon}\right)^3}{K_5+K_6C_\mu\left(\frac{Sk}{\varepsilon}\right)^2+K_7C_\mu^2\left(\frac{Sk}{\varepsilon}\right)^4+K_8\left(\frac{Wk}{\varepsilon}\right)^2} \tag{A.4}$$

where

$$S=\sqrt{2S_{ij}S_{ij}} \tag{A.5}$$

$$W=\sqrt{2W_{ij}W_{ij}} \tag{A.6}$$

Modified flow rotation term

$$W=\left|S\cdot\left(1-\frac{C_4-4}{C_4-2}\right)+\Omega\cdot\left(\frac{C_4-4}{C_4-2}\right)\right| \tag{A.7}$$

where the relative *fluid* rotation-rate magnitude computed in an inertial frame is:

$$\Omega=\sqrt{2\Omega_{ij}\Omega_{ij}} \tag{A.8}$$

Turbulent stresses (Boussinesq's assumption)

$$-\overline{\bar{\rho}u_i u_j} = 2\mu_T S_{ij} - \frac{2}{3}\delta_{ij}\left(\mu_T \frac{\partial U_k}{\partial x_k} + \bar{\rho}k\right) \tag{A.9}$$

Model turbulence length scale

$$L_T = \mathrm{MIN}\left(\frac{C_L y, k^{3/2}}{\varepsilon}\right) \tag{A.10}$$

Near-wall turbulence dissipation rate

The following equations are used only when $C_L y$ is the minimum length scale in Equation (A.10).

$$\varepsilon = \frac{k^{3/2}}{l_\varepsilon} \tag{A.11}$$

$$l_\varepsilon = C_L y\left[1 - \exp\left(\frac{-\mathrm{Re}_y}{A_\varepsilon}\right)\right] \tag{A.12}$$

Near-wall turbulent viscosity

The following equation is used only when C_Ly is the minimum length scale in Equation (A.10):

$$\mu_T = C_\mu \bar{\rho}\sqrt{k} \cdot C_L y\left[1 - \exp\left(\frac{-\mathrm{Re}_y}{A_\mu}\right)\right] \tag{A.13}$$

where

$$\mathrm{Re}_y = \frac{\sqrt{k} \cdot y}{\nu}. \tag{A.14}$$

Model constants

Constants in new turbulence model are given in Table AI.

Detailed derivation of model equations

The development of Equations (13), (15) and (19) in the text are outlined here in more detail. The starting point for the new eddy-viscosity formulation is the explicit algebraic stress formulation of Gatski and Speziale (1993), who derived an expression for the Reynolds-stress anisotropy tensor (Equation (4)). This equation is first linearized with respect to the mean strain-rate tensor to yield:

$$b_{ij} = \frac{\left(\frac{4}{3} - C_2\right)}{(C_3 - 2)} \cdot \frac{6}{3 - 2\eta^2 + 6\zeta^2} \cdot S^*_{ij}. \tag{A.15}$$

Incorporating the definition of the normalized strain-rate S^*_{ij} (Equation (7)), this may be expressed:

Pr_k	1.0
Pr_ε	1.19
$C_{\varepsilon 1}$	1.44
$C_{\varepsilon 2}$	1.92
K_1	0.66
K_2	3.9
K_3	1.0
K_4	5.3
K_5	2.9
K_6	17.0
K_7	10.0
K_8	3.84
C_4	0.4
C_L	2.495
A_ε	4.99
A_μ	25.0

Table AI.
Constants in new turbulence model

$$b_{ij} = \frac{\left(\frac{4}{3} - C_2\right)}{(C_3 - 2)} \cdot \frac{6}{3 - 2\eta^2 + 6\zeta^2} \cdot \frac{(2 - C_3)}{2} \cdot g \cdot \frac{k}{\varepsilon} S_{ij} \tag{A.16}$$

and simplified to:

$$b_{ij} = -\frac{6\left(\frac{4}{3} - C_2\right)}{6 - 4\eta^2 + 12\zeta^2} \cdot g \cdot \frac{k}{\varepsilon} S_{ij}. \tag{A.17}$$

The anisotropy tensor definition for a linear eddy-viscosity model (Equation (2)) may be expressed as:

$$b_{ij} = -\frac{2\mu_T}{\rho k} S_{ij}, \tag{A.18}$$

and incorporating the definition of the eddy viscosity (Equation (3)) with a damping function of unity ($f_\mu = 1$) yields:

$$b_{ij} = -2C_\mu \frac{k}{\varepsilon} S_{ij}. \tag{A.19}$$

Equations (A.17) and (A.19) are combined to yield:

$$C_\mu = \frac{3\left(\frac{4}{3} - C_2\right)}{\left(6 - 4\eta^2 + 12\zeta^2\right)} \cdot g. \tag{A.20}$$

Finally, substitution of the definition of g (Equation (10)) yields the form expressed in Equation

(13):

$$C_\mu = \frac{(4 - 3C_2)}{\left(6 - 4\eta^2 + 12\zeta^2\right)\left[\left(\frac{C_1}{2} - 1\right) + \frac{P^k}{\varepsilon}\right]}. \tag{13}$$

The relation expressed in Equation (13) is next manipulated to develop the implicit expression for eddy viscosity proposed here (Equation (15)). First, the definitions of η^2 and ζ^2 may be expressed in terms of the (non-normalized) strain-rate magnitude (S) and modified rotation-rate magnitude (W):

$$\eta^2 = \frac{(2 - C_3)^2}{8} \cdot g^2 \cdot \frac{k^2}{\varepsilon^2} \cdot S^2 \tag{A.21}$$

$$\zeta^2 = \frac{(2 - C_4)^2}{8} \cdot g^2 \cdot \frac{k^2}{\varepsilon^2} \cdot W^2. \tag{A.22}$$

Substitution into Equation (A.20) yields:

$$C_\mu = \frac{3\left(\frac{4}{3} - C_2\right) \cdot g}{\left[6 - \frac{1}{2}(2 - C_3)^2 \cdot g^2 \cdot \left(\frac{Sk}{\varepsilon}\right)^2 + \frac{3}{2}(2 - C_4)^2 \cdot g^2 \cdot \left(\frac{Wk}{\varepsilon}\right)^2\right]} \tag{A.23}$$

which may be rearranged to:

$$\frac{6}{g^2} \cdot C_\mu - \frac{1}{2}(2 - C_3)^2 \cdot \left(\frac{Sk}{\varepsilon}\right)^2 \cdot C_\mu + \frac{3}{2}(2 - C_4)^2 \cdot \left(\frac{Wk}{\varepsilon}\right)^2 \cdot C_\mu = \frac{3}{g}\left(\frac{4}{3} - C_2\right). \tag{A.24}$$

The pressure strain model on which this formulation is based (Speziale *et al.*, 1991) uses a form of the coefficient C_1 that is linear with respect to the production-to-dissipation ratio, i.e.

$$C_1 = C_{1a} + C_{1b}\frac{P^k}{\varepsilon}, \tag{A.25}$$

in which case g (Equation (10)) can be expressed:

$$g = \left[\left(\frac{1}{2}C_{1a} - 1\right) + \left(\frac{1}{2}C_{1b} + 1\right)\frac{P^k}{\varepsilon}\right]^{-1}. \tag{A.26}$$

The pressure strain model similarly uses a form of the coefficient C_2 of the form:

$$C_2 = C_{2a} - C_{2b}\sqrt{b_{ij}b_{ij}}. \tag{A.27}$$

For the linear model form used here summarized by Equations (2) and (3), the coefficient is equivalently expressed:

$$C_2 = C_{2a} - C_{2b}\frac{1}{\sqrt{2}} \cdot C_\mu\left(\frac{Sk}{\varepsilon}\right). \tag{A.28}$$

Substitution of Equations (A.26) and (A.28) into Equation (A.24) yields:

$$
\begin{aligned}
&6\left(\frac{1}{2}C_{1a}-1\right)^2\cdot C_\mu+12\left(\frac{1}{2}C_{1a}-1\right)\left(\frac{1}{2}C_{1b}+1\right)\cdot\frac{P^k}{\varepsilon}\cdot C_\mu\\
&\quad+6\left(\frac{1}{2}C_{1b}+1\right)^2\cdot\left(\frac{P^k}{\varepsilon}\right)^2\cdot C_\mu-\frac{1}{2}(2-C_3)^2\cdot\left(\frac{Sk}{\varepsilon}\right)^2\cdot C_\mu+\frac{1}{2}(2-C_4)^2\cdot\left(\frac{Wk}{\varepsilon}\right)^2\cdot C_\mu\\
&=3\left(\frac{4}{3}-C_{2a}\right)\left(\frac{1}{2}C_{1a}-1\right)+\frac{3}{\sqrt{2}}C_{2b}\left(\frac{1}{2}C_{1a}-1\right)\cdot\left(\frac{Sk}{\varepsilon}\right)\cdot C_\mu\\
&\quad+3\left(\frac{4}{3}-C_{2a}\right)\left(\frac{1}{2}C_{1b}+1\right)\cdot\frac{P^k}{\varepsilon}+\frac{3}{\sqrt{2}}C_{2b}\left(\frac{1}{2}C_{1b}+1\right)\cdot\frac{P^k}{\varepsilon}\cdot\left(\frac{Sk}{\varepsilon}\right)\cdot C_\mu
\end{aligned}
\tag{A.29}
$$

The turbulence production-to-dissipation ratio may be expressed in terms of the turbulent viscosity coefficient and the dimensionless strain-rate magnitude (Equation (14)). Substitution yields:

$$
\begin{aligned}
&6\left(\frac{1}{2}C_{1a}-1\right)^2\cdot C_\mu+12\left(\frac{1}{2}C_{1a}-1\right)\left(\frac{1}{2}C_{1b}+1\right)\cdot C_\mu^2\cdot\left(\frac{Sk}{\varepsilon}\right)^2\\
&\quad+6\left(\frac{1}{2}C_{1b}+1\right)^2\cdot C_\mu^3\cdot\left(\frac{Sk}{\varepsilon}\right)^4-\frac{1}{2}(2-C_3)^2\cdot\left(\frac{Sk}{\varepsilon}\right)^2\cdot C_\mu+\frac{1}{2}(2-C_4)^2\cdot\left(\frac{Wk}{\varepsilon}\right)^2\cdot C_\mu\\
&=3\left(\frac{4}{3}-C_{2a}\right)\left(\frac{1}{2}C_{1a}-1\right)+\frac{3}{\sqrt{2}}C_{2b}\left(\frac{1}{2}C_{1a}-1\right)\cdot\left(\frac{Sk}{\varepsilon}\right)\cdot C_\mu\\
&\quad+3\left(\frac{4}{3}-C_{2a}\right)\left(\frac{1}{2}C_{1b}+1\right)\cdot C_\mu\cdot\left(\frac{Sk}{\varepsilon}\right)^2+\frac{3}{\sqrt{2}}C_{2b}\left(\frac{1}{2}C_{1b}+1\right)\cdot C_\mu^2\cdot\left(\frac{Sk}{\varepsilon}\right)^3
\end{aligned}
\tag{A.30}
$$

To obtain the implicit form for C_μ, the sole negative term in Equation (A.30) is removed by adding $\frac{1}{2}(2-C_3)^2\cdot\left(\frac{Sk}{\varepsilon}\right)^2\cdot C_\mu$ to both sides, so that it may be equivalently expressed:

$$
\begin{aligned}
&\left[6\left(\frac{1}{2}C_{1a}-1\right)^2+12\left(\frac{1}{2}C_{1a}-1\right)\left(\frac{1}{2}C_{1b}+1\right)\cdot C_\mu\cdot\left(\frac{Sk}{\varepsilon}\right)^2\right.\\
&\quad\left.+6\left(\frac{1}{2}C_{1b}+1\right)^2\cdot C_\mu^2\cdot\left(\frac{Sk}{\varepsilon}\right)^4+\frac{1}{2}(2-C_4)^2\cdot\left(\frac{Wk}{\varepsilon}\right)^2\right]\cdot C_\mu\\
&=3\left(\frac{4}{3}-C_{2a}\right)\left(\frac{1}{2}C_{1a}-1\right)+\frac{3}{\sqrt{2}}C_{2b}\left(\frac{1}{2}C_{1a}-1\right)\cdot\left(\frac{Sk}{\varepsilon}\right)\cdot C_\mu+\frac{1}{2}(2-C_3)^2\cdot\left(\frac{Sk}{\varepsilon}\right)^2\cdot C_\mu\\
&\quad+3\left(\frac{4}{3}-C_{2a}\right)\left(\frac{1}{2}C_{1b}+1\right)\cdot C_\mu\cdot\left(\frac{Sk}{\varepsilon}\right)^2+\frac{3}{\sqrt{2}}C_{2b}\left(\frac{1}{2}C_{1b}+1\right)\cdot C_\mu^2\cdot\left(\frac{Sk}{\varepsilon}\right)^3
\end{aligned}
\tag{A.31}
$$

Finally, the bracketed expression on the left-hand side of Equation (A.31) is divided through to yield the expression for C_μ:

$$C_\mu = \frac{K_1 + K_2 C_\mu \left(\frac{Sk}{\varepsilon}\right)^2 + K_3 C_\mu \left(\frac{Sk}{\varepsilon}\right) + K_4 C_\mu^2 \left(\frac{Sk}{\varepsilon}\right)^3}{K_5 + K_6 C_\mu \left(\frac{Sk}{\varepsilon}\right)^2 + K_7 C_\mu^2 \left(\frac{Sk}{\varepsilon}\right)^4 + K_8 \left(\frac{Wk}{\varepsilon}\right)^2} \tag{15}$$

where, for example, the constant K_1 is expressed in terms of the original model constants as:

$$K_1 = 3\left(\frac{4}{3} - C_{2a}\right)\left(\frac{1}{2}C_{1a} - 1\right). \tag{A.32}$$

As discussed in the text, the flow rotation rate used to incorporate rotational/curvature effects in to the model is obtained approximately, by consideration of the special case of a two-dimensional shear layer rotating with angular velocity ω_m. For such a case, the velocity gradient tensor expressed in a frame with rotation rate ω_m is:

$$\frac{\partial U_i}{\partial x_j} = \begin{bmatrix} 0 & S \\ 0 & 0 \end{bmatrix}, \tag{A.33}$$

and the strain-rate and rotation-rate tensors (in the rotating frame) are:

$$S_{ij} = \begin{bmatrix} 0 & S/2 \\ S/2 & 0 \end{bmatrix} \tag{A.34}$$

$$\Omega'_{ij} = \begin{bmatrix} 0 & S/2 \\ S/2 & 0 \end{bmatrix}. \tag{A.35}$$

In an inertial frame, the rotation-rate tensor is expressed:

$$\Omega_{ij} = \begin{bmatrix} 0 & S/2 - \omega_m \\ -S2 + \omega_m & 0 \end{bmatrix}. \tag{16}$$

A flow rotation rate of $\omega_m = \frac{S}{2}$ implies the limiting case of irrotational flow, occurring for example in an ideal vortex. For rotation rates less than or equal to this value, representative of a rotating shear layer, the flow rotation rate ω_m may be computed as a function of the strain rate and rotation rate expressed in an inertial frame. It is apparent that the rotation-rate magnitude (in an inertial frame) is equal to:

$$\Omega \equiv \sqrt{2\Omega_{ij}\Omega_{ij}} = S - 2\omega_m. \tag{A.36}$$

This expression is rearranged to yield the flow rotation rate in terms of the strain-rate magnitude and the inertial frame rotation-rate magnitude:

$$\omega_m = \frac{1}{2} \cdot (S - \Omega). \tag{A.37}$$

Substituting this into the expression for the modified rotation-rate tensor used to compute C_μ (Equation (9)) yields:

$$W_{12} = -W_{21} = \frac{S}{2} - \frac{(C_4 - 4)}{(C_4 - 2)} \cdot \frac{1}{2} \cdot (S - \Omega). \tag{A.38}$$

The modified rotation-rate magnitude ($W = \sqrt{2W_{ij}W_{ij}}$) is then computed to be

$$W = \left| S \cdot \left(1 - \frac{C_4 - 4}{C_4 - 2} \right) + \Omega \cdot \left(\frac{C_4 - 4}{C_4 - 2} \right) \right| = \left| \frac{9}{4}\Omega - \frac{5}{4}S \right|. \tag{19}$$

As discussed above, this formulation is frame indifferent, and provides an approximation of the flow rotation rate, defined as the Lagrangian rate of rotation of the principal axes of the strain-rate tensor.

Corresponding author
D. Keith Walters can be contacted at: walters@me.msstate.edu